EUROPEAN ORGANIZATION FOR NUCLEAR RESEARCH

Proposal to the ISOLDE and Neutron Time-of-Flight Committee

(Following HIE-ISOLDE Letter of Intent I-169)

Complementary measurements of octupole collectivity in ^{146}Ce

May 13, 2021

L. P. Gaffney[1], M. Au[2], M. Beckers[3], A. Briscoe[4], P. A. Butler[1], A. Dolan[1], Ch. Fransen[3], S. J. Freeman[5], A. B. Garnsworthy[6], P. E. Garrett[7], K. Hadyńska-Klęk[8], J. Henderson[9], C. Henrich[10], A. Illana[4], D. T. Joss[1], A. Jungclaus[11], D. Kalaydjieva[12], B. Kay[13], M. Komorowska[8], W. Korten[12], Th. Kröll[10], M. Labiche[14], I. Lazarus[14], Z. P. Li[15], A. Montes Plaza[4], P. Napiorkowski[8], B. S. Nara Singh[16], K. Nomura[17], D. O'Donnell[16], J. Ojala[4], B. Olaizola[2], R. D. Page[1], J. Pakarinen[4], P. Papadakis[14], R. Raabe[18], L. Robledo[19], M. Rocchini[7], S. Rothe[2], M.-M. Satrazani[1], M. Scheck[16], D. K. Sharp[5], J. Smallcombe[1], J. F. Smith[16], P. Spagnoletti[20], S. Stegemman[2], T. Stora[2], W. Sun[15], N. Warr[3], K. Wrzosek-Lipska[8], M. Zielińska[12]

[1] *University of Liverpool, UK*
[2] *CERN-ISOLDE, Switzerland*
[3] *Universität zu Köln, Germany*
[4] *University of Jyvaskyla, Finland*
[5] *The University of Manchester, UK*
[6] *TRIUMF, Canada*
[7] *University of Guelph, Canada*
[8] *University of Warsaw, Poland*
[9] *University of Surrey, UK*
[10] *Technische Universität Darmstadt, Germany*
[11] *Instituto de Estructura de la Materia, CSIC, Spain*
[12] *IRFU CEA, Université Paris-Saclay, France*
[13] *Argonne National Laboratory, USA*
[14] *STFC Daresbury Laboratory, UK*
[15] *Southwest University, China*
[16] *University of the West of Scotland, UK*
[17] *University of Zagreb, Croatia*
[18] *KU Leuven, Belgium*
[19] *Universidad Autónoma de Madrid, Spain*
[20] *Simon Fraser University, Canada*

CERN-INTC-2021-040 / INTC-P-609
13/05/2021

Spokespersons: L. P. Gaffney [liam.gaffney@liverpool.ac.uk]
Contact person: B. Olaizola [bruno.olaizola@cern.ch]

Abstract: We are proposing to study octupole collectivity in ^{146}Ce using the complementary techniques of Coulomb excitation and inelastic scattering. Using the same HIE-ISOLDE beam at two different energies of 4.2 MeV/u and 7.5 MeV/u, the experiments can be run back-to-back at the neighbouring experimental setups of the Miniball γ-ray Spectrometer and the ISOLDE Solenoidal Spectrometer (ISS). The aim of these measurements is to determine the $B(E3; 0_1^+ \rightarrow 3_1^-)$ and $B(E3; 2_1^+ \rightarrow 5_1^-)$ values in isotopes where octupole correlations are expected to be present in the ground-state structures. For the former, we plan to take advantage of the (d, d') reaction at ISS, which negates the use of γ-ray detection, overcoming sensitivity constraints experienced in this region for the measurement of $B(E3)$ values so far. Combining this with the nuclear-model-independent technique of Coulomb excitation using Miniball not only serves as a test of this new method, but also simultaneously gives access to a range of other $E2$ and $E3$ transition strengths that help understand the nature of the octupole collectivity in the lanthanide region.

Requested shifts: 17 shifts, (split into 1 runs over 1 years)
Installations: ISS with Si array and ionisation chamber + Miniball with CD

1 Physics Case

Octupole collectivity: Octupole collectivity has been noted around $Z = 56, N = 88$ for some time [1–3] and low-lying negative-parity bands are known in the heavy cerium isotopes [4–7]. The shell structure of these nuclei allow for excitations of both protons and neutrons between single-particle orbitals that have opposite parity and $\Delta j = \Delta l = 3$, thought to drive this enhancement of octupole correlations [8]. Studying the electromagnetic properties of excited states in nuclei with octupole correlations is crucial to understanding such a subtle interplay [9, 10]. New calculations going beyond the mean-field are proving to be the most reliable way of making predictions about octupole states in the actinide region [11–14] and now also in the lanthanide region [15, 16]. The most recent global analysis of ground-state properties using covariant density functional theory shows how important ^{148}Ce is in this context [17]. In these calculations, a minimum is predicted in the potential energy surface at $\beta_3 = 0.125$ for ^{148}Ce, with a gain in binding energy of more than 700 keV due to the octupole deformation, the largest in the region. Hartree-Fock plus BCS calculations using realistic Gogny forces [18] have also been carried out in the lanthanide region and predict a maximum in octupole deformation for ^{146}Ce, with $\beta_3 = 0.139$. Use of the IBM in combination with microscopic energy density functional theory [19, 20] has a lot of success reproducing $B(E3)$ values in both the actinide and lanthanide regions and allows for predictions for a complete set of electromagnetic matrix elements. A summary of the theoretical predictions for $B(E3; 0_1^+ \rightarrow 3_1^-)$ values in the lanthanide region is presented in Fig. 1.

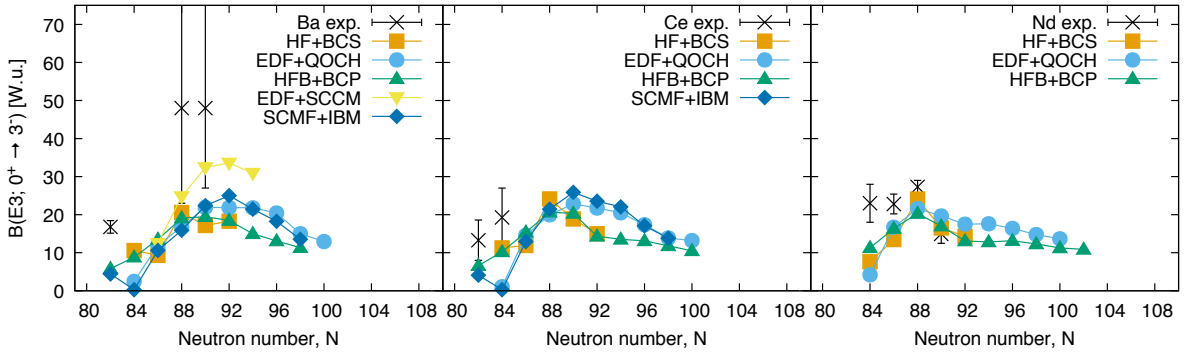

Figure 1: $B(E3; 0_1^+ \rightarrow 3_1^-)$ values in the neutron-rich Ba ($Z = 56$), Ce ($Z = 58$), and Nd ($Z = 60$) isotopic chains. Experimental data from Refs [21–23] plus NNDC are shown in black. Five different theoretical predictions currently available in the literature are also shown; Ref. [18, 24] in orange, Ref. [25] in light blue, Refs. [26] in green, Ref. [15] in yellow and Ref. [19, 20] in dark blue.

Experimental data in the lanthanide region: Recently, experimental data were obtained for ^{144,146}Ba [21, 22], showing indication of an enhanced octupole collectivity beyond that predicted by state-of-the-art models, albeit the low precision shows consistency with theory at the lower limit. In order to investigate any claims of enhancement in the $B(E3)$ values in this region of the nuclear chart, systematic and precise data are required. Studying octupole collectivity with Coulomb excitation at ISOLDE has now been established

with experiments in the actinide region [27–29] and the first steps in the lanthanide region were successfully made in 2017 and 2018 with ^{142}Xe [30] and ^{142,144}Ba [23]. Preliminary results from the ^{142}Ba analysis indicate that the $B(E3)$ value is not enhanced to the same degree as the heavier neighbouring isotopes, although the precision is much improved. The ^{144}Ba experiment suffered from a failed target unit and only a limited amount of the proposed total statistics were measured; the remaining shifts have been carried forward after LS2. A further detailed investigation of octupole collectivity in ^{144,145}Ba is the aim of accepted proposal IS656 [31].

Coulomb excitation vs. inelastic scattering: We are proposing to explore a complementary technique to Coulomb excitation, that of nuclear inelastic scattering using deuterons as an isoscalar probe, i.e. (d, d'). This technique has been performed routinely in normal kinematics with deformed rare-earth nuclei since the 1960's [32–37] and this current proposal will extend this to inverse kinematics systems by exploiting the resolving power of the ISS. Radioactive targets have also been employed with this method for the study of octupole excitations in ^{226}Ra [38], ^{246,248}Cm [39] and ^{250}Cf [40]. We will measure excited-state populations following the (d, d') reaction, detecting the scattered deuterons in the forwards laboratory angles, making coincidences with recoils in the new gas ionisation chamber. The proposed method avoids the issues around detection of weak γ-ray branches and feeding history so far experienced in Coulomb-excitation experiments in this region of the nuclear chart.

Cross-sections for (d, d') are smaller than those for Coulomb excitation, but become competitive when detection efficiency is taken in to account. Both techniques are sensitive to $E2$ and $E3$ transitions and as such are ideal probes of quadrupole-octupole collectivity. Furthermore, single-step excitations are strongly preferred in this higher energy technique using light ions, giving a complementary set of data to the multi-step process of Coulomb excitation. We believe that combining these techniques is a method perfectly suited to obtain precision $E3$ transition moments in the lanthanide region, not just from the ground state, i.e. $B(E3; 0^+ \rightarrow 3^-)$, but also multi-step transitions that can give key information on the dynamic nature of the collectivity, such as $B(E3; 2^+ \rightarrow 1^-)$ and $B(E3; 2^+ \rightarrow 5^-)$ [41].

Optical models are required for the interpretation of (d, d') cross-section data, allowing for the extraction of the deformation length, β_λ, under the assumption that the charge and matter distributions are coupled in a deformed nucleus [37, 42]. This model-dependent analysis introduces systematic uncertainties due to the choice of optical model parameters and the finite range of the DWBA calculations. A convenient test of the model comes from the known $B(E2)$ value for populating the 2^+_1, which is simultaneously measured in this experiment, as well as the elastic scattering channel. Efforts to accurately quantify these uncertainties in (d, p) reactions are more advanced [43] than for (d, d'), although a large quantity of elastic scattering data is available [44] to constrain global fits [45]. Detailed analysis of high statistics ^{94}Mo data was able to constrain model uncertainties to 5% for $B(E2)$ values [46]. Systematic uncertainties in the extraction of $B(E3)$ might be expected to be as large as 10 – 20% [40], which can be estimated in the final analysis by varying the choice of optical model parameters, constrained by elastic scattering data in the region and the higher statistics 2^+ excitation obtained in this same measurement.

The current lack of precision data in the neutron-rich Ba-Ce nuclei make these good candidates for the first exploration of this complementary technique. We are proposing to begin with ^{146}Ce, with a view to a larger campaign in the future of isotopes in this region; later extending the technique to the actinide region of the nuclear chart. This choice is motivated by the availability of recently obtained and extensive β-decay data from the GRIFFIN spectrometer at TRIUMF [47], which helps to constrain the Coulomb-excitation part of the measurement. In addition, ^{146}Ce is well suited to (d, d') due to the large energy separation of the excited 2^+ (258 keV) and 3^- (961 keV) states and recent beam development at ISOLDE created a unique opportunity worldwide in this regard.

2 Experiments

Beam production and yields: Isobaric contamination in this region of the nuclear chart is a major problem with ISOL methods, in particular from the strongly ionised Cs isotopes, that are released very quickly from the target. To avoid this, molecular beams have been employed at ISOLDE to great effect [48, 49]. For the cerium isotopes, oxide beams were previously employed [50] and more recently, fluorination tests by TISD were performed during setup of ^{144}Ba^{19}F beam for Miniball [51], following a Letter of Intent for beam development [52]. Yields were measured for ^{A}Ce^{19}F beams at $A = 146$ (1.9×10^7 ions/μC) and $A = 148$ (1.3×10^6 ions/μC), indicating purities of $\approx 60\%$ and $> 90\%$, respectively, with ^{A}La^{19}F being the main contaminant. The original LOI also suggested ^{A}Ce^{19}F$_2$ beams should be investigated to suppress isobaric contamination, but this was not fully tested at the time except to look for ^{144}Ba^{19}F$_2$, which was below the detection limit. As part of this proposal, we are requesting one extra shift in collaboration with TISD to investigate different molecular beams during the setup of the experiment. REX-TRAP/EBIS efficiency is conservatively estimated to be 5%, based upon the observation for ^{144}BaF of $\simeq 10\%$, which used the same molecular breakup process. Charge state selection should be optimised to maximise the beam energy for the inelastic scattering measurement, which may lead to a reduced EBIS efficiency in this case. Transmission through HIE-ISOLDE is assumed to be 70%, giving a total post-acceleration efficiency of 3.5%. At an average proton current of 1.5 μA, the beam intensity at ISS and Miniball will be 1.0×10^6 ions/s for ^{146}Ce.

Inelastic scattering with ISS: It is proposed to use the ISS with the on-axis silicon array in the downstream configuration, in combination with the fast-counting ionisation chamber. Kinematics simulations have been performed for the ^{146}Ce(d,d') reaction, at a beam energy of 7.5 MeV/u and magnetic field strength of 2.5 T and are shown in the left panel of Fig. 2. A CD_2 target of thickness $\simeq 100$ μg/cm^2 has been assumed and input cross-sections (left panel of Fig. 2) are calculated using the finite-range DWBA code, Ptolemy [53, 54], using global optical-model parameters from Ref. [45]. It is found that the optimal position of the array is at +125 mm, covering the angular range of 22° – 46° in the centre-of-mass frame of reference, indicated by the dashed lines in the right panel of Fig. 2. This covers the maximum of the 3^- state cross-section and is large enough in angle to allow for suppression of the high-rate elastic scattering deuterons. Furthermore, elastic scattering of the beam from the carbon in the target will need to be shielded

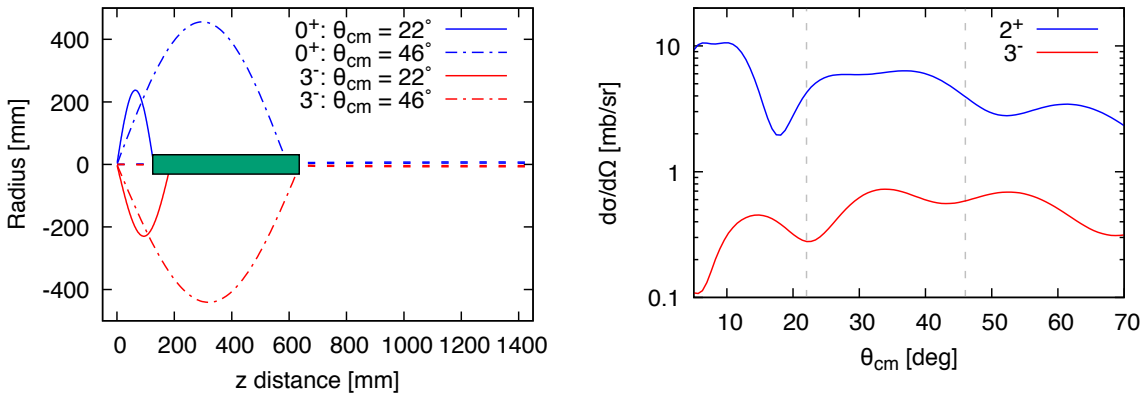

Figure 2: (Left) Kinematics for ^{146}Ce(d, d') in inverse kinematics at 7.5 MeV/u using the ISOLDE Solenoidal Spectrometer with a magnetic field strength of 2.5 T. (Right) Cross-sections for excitation of the first-excited 2^+ and 3^- states using Ptolemy [53, 54], as described in the text. The vertical dashed lines mark the region covered by the on-axis array.

by a moveable 6 mm diameter blocker placed at 1.6 m from the target to reduce the instantaneous rate in the ionisation chamber.

A full simulation of the reaction has been performed using NPTool [55], with the DWBA cross-sections as an input. All simulations assume a beam spot diameter of $\sigma_{x,y} = 0.5$ mm at the target positions, a divergence of $\sigma_\theta = 0.8$ mrad, and an energy spread of $\sigma_E = 0.5\%$. Deuterons at laboratory angles close to 90° can undergo multiple orbits in the solenoidal field before intersecting the on-axis silicon array, i.e. low centre-of-mass angles or small z values. These appear in the left panel of Fig 3 as spurious features and as a background contribution in the right panel showing the excitation energy spectrum. It is to be tested if such events can be distinguished by their measured cyclotron period, $T = 52$ ns for a single orbit, or if they need to be blocked with a collimator at the target position.

In order to achieve a statistical precision in the $B(E3)$ value better than the $\simeq$ 10% systematic uncertainty, at least 500 counts are required across the array. This also gives enough sensitivity to distinguish the angular distribution and confirm the 3^- assignment for this state. The excitation of the 1^- will be at the percent level of the 3^- state, but will not be resolved in the Q-value spectrum. Assuming a value of the transition strength, similar to that recently measured in ^{142}Ba, i.e $B(E3; 0^+ \rightarrow 3^-) \simeq 20$ W.u., and taking in to account the active area of the silicon array (94% in θ and 70% in ϕ), the required level of statistics will be achieved in 7 shifts of beam on target. The total number of counts for the 2^+ excitation in this period will be an order of magnitude larger, allowing for an independent normalisation of the data against a known $B(E2)$ value [47, 56].

Coulomb-excitation with Miniball: It is proposed to perform a "safe" Coulomb-excitation measurement using the standard Miniball setup coupled with the CD detector in the forwards angles. In order to maximise multi-step excitation, giving sensitivity to a complementary set of $E3$ transition matrix elements to the (d, d') measurement, a ^{208}Pb target is chosen and a beam energy of 4.2 MeV/u will be used, close to the safe

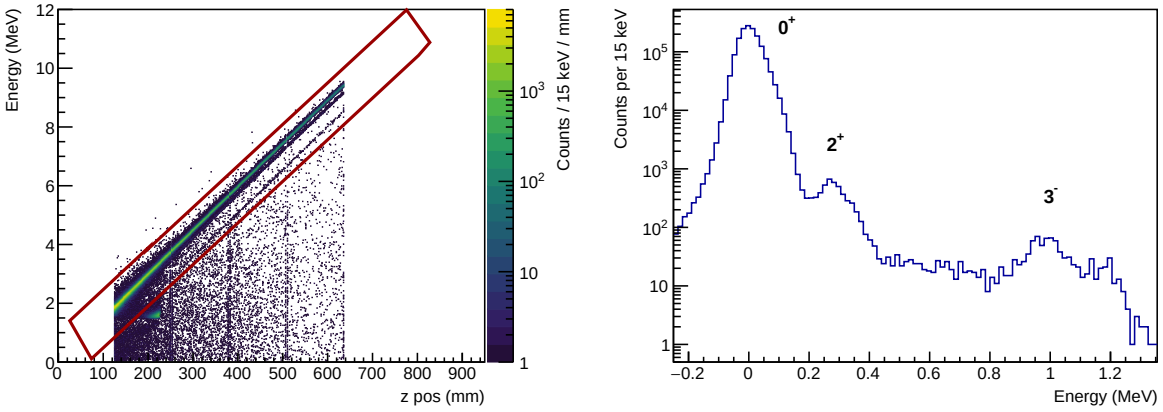

Figure 3: NPTool simulations as described in the text: (Left) Deuteron energy versus z position measured in the on-axis array. (Right) The derived excitation energy spectrum for all events after applying the ROI cut indicated in red in the left panel.

limit. The target thickness is chosen to maximise the number of counts observed, whilst ensuring clean separation of the kinematics in the CD detector, shown in the left panel of Fig. 4. Gosia calculations have been performed to estimate the expected yields, shown in the right side of Fig. 4 for a few selected transitions. Matrix elements were calculated from the collective model assuming a spin-independent value of the intrinsic quadrupole and octupole moments, consistent with the lifetime of the 2_1^+ state [56] and $B(E3; 0_1^+ \rightarrow 3_1^-) = 20$ W.u., respectively. In order to achieve a minimum of 500 counts in the $3_1^- \rightarrow 0_1^+$ transition, we require 7 shifts of beam on target. This will yield more than 1000 total counts in the $5_1^- \rightarrow 2_1^+$ depopulating transition, giving sensitivity from this measurement to the $\langle 2_1^+||E3||5^-\rangle$ and $\langle 4_1^+||E3||5^-\rangle$ matrix elements from the angular distribution of particle-γ events. Furthermore, population of the 1^- state via the $\langle 2_1^+||E3||1^-\rangle$ matrix elements can be obtained from the decaying $E1$ transitions to the ground and 2^+ states. The level scheme shown in the right panel of Fig. 4 does not include the $K = 2$ band or intruder band with band-head energies of 1.274 MeV and 1.043 MeV, respectively. Significant population of these bands is expected, at least of the same order of magnitude as the negative-parity band, depending on the magnitude of the inter-band transition strengths, to which this experiment will be sensitive. The use of γ-ray branching ratio data in combination with the Coulomb-excitation yields is important to constrain the fit of matrix elements and determine possible feeding to the negative-parity states. The complementary experiments recently performed with the GRIFFIN spectrometer at TRIUMF [47] provides this data with high precision.

Summary of requested shifts: We are requesting a total of **17 shifts**:

- ISS: **8 shifts**; 7 shifts for the (d, d') measurement plus 1 for optimisation of beam tuning in to the setup and positioning of the blocker.
- Miniball: **7 shifts** for the Coulomb-excitation measurement.
- Beam-energy and beam-line change: **1 shift**.
- TISD: **1 shift** to optimise molecular beam production and yield measurements.

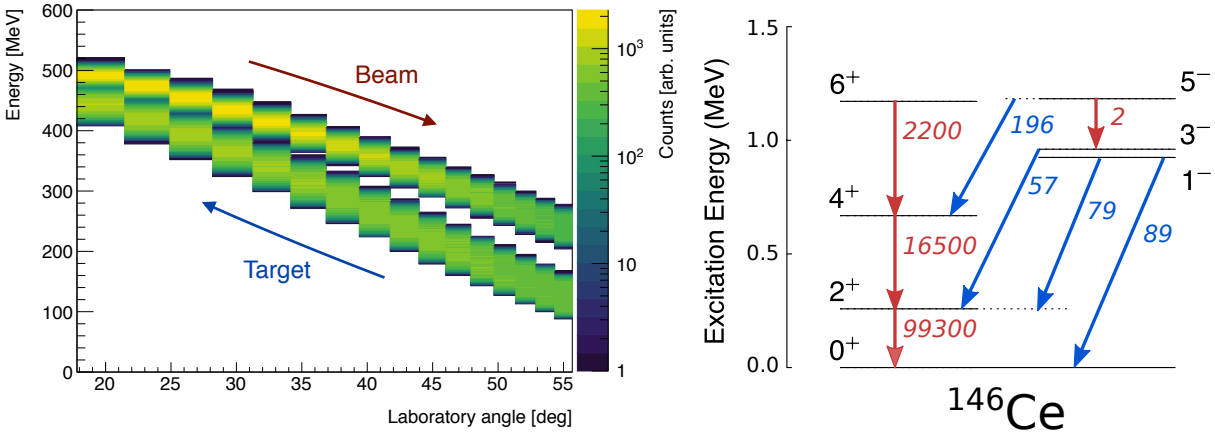

Figure 4: Coulomb-excitation simulations: (Left) Kinematics simulations [57] of a ^{146}Ce beam at 4.2 MeV/u on a 2.0 mg/cm^2 thick ^{208}Pb target, with the CD detector placed at a distance of 28.0 mm. Clear separability of the scattered beam and recoiling projectile is demonstrated. The arrows indicate the direction of increasing centre of mass angles, covering from 32° to 144°. (Right) Partial level scheme of ^{146}Ce showing yields (per shift) of depopulating $E2$ (red) and $E1$ (blue) transitions obtained from Gosia calculations [58, 59], as described in the text. Excitations proceed via $E2$ and $E3$ transitions from the ground state.

References

[1] G. A. Leander et al., Nucl. Phys. A **388**, 452 (1982).
[2] P. A. Butler and W. Nazarewicz, Nucl. Phys. A **533**, 249 (1991).
[3] P. A. Butler and W. Nazarewicz, Rev. Mod. Phys. **68**, 349 (1996).
[4] W. Phillips et al., Phys. Lett. B **212**, 402 (1988).
[5] J. Hamilton et al., Prog. Part. Nucl. Phys. **35**, 635 (1995).
[6] S. Zhu et al., Phys. Lett. B **357**, 273 (1995).
[7] Y. Chen et al., Phys. Rev. C **73**, 054316 (2006).
[8] P. A. Butler, J. Phys. G Nucl. Part. Phys. **43**, 073002 (2016).
[9] L. M. Robledo and P. A. Butler, Phys. Rev. C **88**, 051302 (2013).
[10] M. Chen, T. Li, J. Dobaczewski, and W. Nazarewicz, Phys. Rev. C **103**, 034303 (2021).
[11] L. M. Robledo and G. F. Bertsch, Phys. Rev. C **84**, 54302 (2011).
[12] J. M. Yao, E. F. Zhou, and Z. P. Li, Phys. Rev. C **92**, 041304 (2015).
[13] Z. P. Li, T. Nikšić, and D. Vretenar, J. Phys. G Nucl. Part. Phys. **43**, 024005 (2016).
[14] K. Nomura, R. Rodríguez-Guzmán, L. M. Robledo, and J. E. García-Ramos, Phys. Rev. C **103**, 2101.02982 (2021).
[15] R. N. Bernard, L. M. Robledo, and T. R. Rodríguez, Phys. Rev. C **93**, 061302 (2016).
[16] K. Nomura, L. Lotina, T. Nikšić, and D. Vretenar, Phys. Rev. C **103**, 054301 (2021).
[17] S. E. Agbemava, A. V. Afanasjev, and P. Ring, Phys. Rev. C **93**, 044304 (2016).
[18] J. Egido and L. Robledo, Nucl. Phys. A **545**, 589 (1992).
[19] K. Nomura, D. Vretenar, T. Nikšić, and B.-N. Lu, Phys. Rev. C **89**, 024312 (2014).
[20] K. Nomura, T. Nikšić, and D. Vretenar, Phys. Rev. C **97**, 024317 (2018).

[21] B. Bucher et al., Phys. Rev. Lett. **116**, 112503 (2016).
[22] B. Bucher et al., Phys. Rev. Lett. **118**, 152504 (2017).
[23] M. Scheck and D. T. Joss, CERN-INTC **047**, 348 (2012).
[24] J. Egido and L. Robledo, Nucl. Phys. A **518**, 475 (1990).
[25] S. Y. Xia et al., Phys. Rev. C **96**, 054303 (2017).
[26] L. M. Robledo, M. Baldo, P. Schuck, and X. Viñas, Phys. Rev. C **81**, 034315 (2010).
[27] L. P. Gaffney et al., Nature **497**, 199 (2013).
[28] P. A. Butler et al., Nat. Commun. **10**, 2473 (2019).
[29] P. A. Butler et al., Phys. Rev. Lett. **124**, 042503 (2020).
[30] C. Henrich et al., Acta Phys. Pol. B **49**, 529 (2018).
[31] T. Braunroth et al., CERN-INTC **091**, 530 (2017).
[32] B. Zeidman, B. Elbek, B. Herskind, and M. Olesen, Nucl. Phys. **86**, 471 (1966).
[33] E. Veje, B. Elbek, B. Herskind, and M. Olesen, Nucl. Phys. A **109**, 489 (1968).
[34] T. Grotdal, K. Nybø, T. Thorsteinsen, and B. Elbek, Nucl. Phys. A **110**, 385 (1968).
[35] N. Trautner, G. Løvhøiden, and P. Christensen, Phys. Lett. B **44**, 41 (1973).
[36] F. Štěrba, Czechoslov. J. Phys. **31**, 578 (1981).
[37] I. M. Govil et al., Phys. Rev. C **33**, 793 (1986).
[38] T. F. Thorsteinsen, K. Nybø, and G. Løvhøiden, Phys. Scr. **42**, 141 (1990).
[39] S. W. Yates, A. M. Friedman, and I. Ahmad, Phys. Rev. C **12**, 795 (1975).
[40] I. Ahmad, A. M. Friedman, and S. W. Yates, Phys. Rev. C **21**, 874 (1980).
[41] R. Ibbotson et al., Phys. Rev. Lett. **71**, 1990 (1993).
[42] W. T. Pinkston and G. R. Satchler, Nucl. Phys. **27**, 270 (1961).
[43] G. B. King, A. E. Lovell, and F. M. Nunes, Phys. Rev. C **98**, 44623 (2018).
[44] C. Perey and F. Perey, At. Data Nucl. Data Tables **17**, 1 (1976).
[45] W. W. Daehnick, J. D. Childs, and Z. Vrcelj, Phys. Rev. C **21**, 2253 (1980).
[46] J. L. Duarte, G. M. Ukita, T. Borello-Lewin, L. B. Horodynski-Matsushigue, and L. C. Gomes, Phys. Rev. C - Nucl. Phys. **56**, 1855 (1997).
[47] L. P. Gaffney, A. B. Garnsworthy, P. E. Garrett, and Others, Propososal to TRIUMF EEC , S1626 (2015).
[48] R. Eder et al., Nucl. Instrum. Meth. B **62**, 535 (1992).
[49] U. Köster et al., Eur. Phys. J. Spec. Top. **150**, 285 (2007).
[50] H.-J. Kluge, *Isolde Users' Guide*, CERN, Geneva, 1986.
[51] S. Rothe, ISOLDE Oper. Logb. (2017).
[52] L. P. Gaffney et al., CERN-INTC **032**, 169 (2016).
[53] M. Macfarlane and S. Pieper, Argonne Natl. Lab. Reports **76**, 11 (1978).
[54] M. Rhoades-Brown, M. H. MacFarlane, and S. C. Pieper, Phys. Rev. C **21**, 2436 (1980).
[55] A. Matta et al., J. Phys. G Nucl. Part. Phys. **43**, 045113 (2016).
[56] H. Mach, R. L. Gill, and M. Moszyński, Nucl. Inst. Methods Phys. Res. A **280**, 49 (1989).
[57] L. P. Gaffney, lpgaff/kinsim: kinsim: A kinematics simulator for Coulomb-excitation experiments using the Miniball CD detector, 2021.
[58] T. Czosnyka, D. Cline, and C. Y. Wu, Bull. Am. Phys. Soc. **28**, 745 (1983).
[59] M. Zielińska et al., Eur. Phys. J. A **52**, 99 (2016).

Appendix

DESCRIPTION OF THE PROPOSED EXPERIMENT

The experimental setup comprises: *The ISOLDE Solenoidal Spectrometer* and *Miniball*

Part of the	Availability	Design and manufacturing
ISOLDE Solenoidal Spectrometer	☒ Existing	☒ To be used without any modification ☐ To be modified
	☐ New	☐ Standard equipment supplied by a manufacturer ☐ CERN/collaboration responsible for the design and/or manufacturing
Miniball + CD	☒ Existing	☒ To be used without any modification ☐ To be modified
	☐ New	☐ Standard equipment supplied by a manufacturer ☐ CERN/collaboration responsible for the design and/or manufacturing

HAZARDS GENERATED BY THE EXPERIMENT (if using fixed installation:) Hazards named in the document relevant for the fixed ISS installation and the fixed Miniball installation.

Additional hazards:

Hazards	ISS	Miniball	
Thermodynamic and fluidic			
Pressure			
Vacuum			
Temperature			
Heat transfer			
Thermal properties of materials			
Cryogenic fluid			
Electrical and electromagnetic			
Electricity			
Static electricity			
Magnetic field	2.5 T		
Batteries			
Capacitors			
Ionizing radiation			
Target material	Deuterated polyethylene, CD_2 (50-400 $\mu g/cm^2$)	^{208}Pb (2.0 mg/cm^2)	
Beam particle type	^{146}Ce	^{146}Ce	

Beam intensity	1.0×10^6	1.0×10^6	
Beam energy	7.5 MeV/u	4.2 MeV/u	
Cooling liquids			
Gases			
Calibration sources:	☒		
• Open source	☒ (α calibrations source 4236RP)		
• Sealed source			
• Isotope	^{148}Gd, ^{239}Pu, ^{241}Am, ^{244}Cm		
• Activity	1 kBq, 1 kBq, 1 kBq, 1 kBq = 4 kBq		
Use of activated material:			
• Description			
• Dose rate on contact and in 10 cm distance			
• Isotope			
• Activity			
Non-ionizing radiation			
Laser			
UV light			
Microwaves (300MHz-30 GHz)			
Radiofrequency (1-300 MHz)			
Chemical			
Toxic			
Harmful			
CMR (carcinogens, mutagens and substances toxic to reproduction)			
Corrosive			
Irritant			
Flammable			
Oxidizing			
Explosiveness			
Asphyxiant			
Dangerous for the environment			
Mechanical			
Physical impact or mechanical energy (moving parts)			

Mechanical properties (Sharp, rough, slippery)			
Vibration			
Vehicles and Means of Transport			
Noise			
Frequency			
Intensity			
Physical			
Confined spaces			
High workplaces			
Access to high workplaces			
Obstructions in passageways			
Manual handling			
Poor ergonomics			

Hazard identification:

Average electrical power requirements (excluding fixed ISOLDE-installation mentioned above): N/A